

NUMERICAL AND EXPERIMENTAL ANALYSIS OF SEEPAGE BENEATH A MODEL OF A GRAVITY DAM

T. Jelenković – V. Travaš *

Chair of Hydraulic Engineering, Faculty of Civil Engineering, University of Rijeka, Radmile Matejčić 3, Rijeka

ARTICLE INFO

Article history:

Received 17.9.2012

Received in revised form 20.2.2013

Accepted 20.2.2013

Keywords:

Darcy law

Finite difference method

Local erosion

Physical model

Saturated porous media

Steady seepage flow

Abstract:

For a steady flow condition beneath a physical model of a typical gravity dam, a comparative analysis between the measured flow data and the one predicted by numerical analysis is presented. The velocity vector field is compared qualitatively and the pressure field is compared quantitatively (on a relevant sections of the flow domain). The numerical analysis is performed by solving the Laplace differential equation by finite difference method. Finally, a particular interest is dedicated to a velocity field and the process of local erosion.

1 Introduction

Dams are engineering structures built for retaining water. To ensure their static resistance and dynamic stability, it is very important to quantify the seepage, i.e. to analyze the flow field beneath the dam. The above mentioned is important for several reasons [1]: (i) to quantify the pressure load, i.e. buoyancy on the dam foundation, (ii) to reduce the buoyancy under some predefined magnitude by identifying the necessary depth of the hydraulic barrier below the foundation, (iii) to identify the total pressure load on the hydraulic barrier and (iv) to quantify the discharge Q beneath the hydraulic barrier (Fig. 1).

The hydraulic analysis serves also to reveal if there exists a danger of attaining flow conditions that will lead to local erosion [2,3,4]. Namely, the difference in water depth at the upstream and downstream part of the dam induces a flow around the foundation. Particularly, at the downstream part of the dam, i.e. at the tip of the dam foundation, the velocity vectors can be oriented upward (Fig. 2). If in this region the velocity magnitude exceeds the value at which the induced hydrodynamic force on soil particles

become equal or greater than the gravity force, the soil particles will be lifted apart and dispersed. As a consequence, the soil bearing capacity could be vanished. To prevent such a scenario the flow field should be adequately manipulated by embedding hydraulic barriers [5].

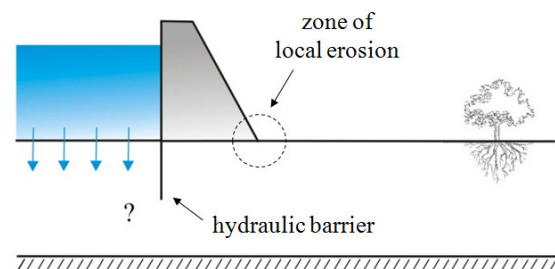


Figure 1. Cross section of a typical gravity dam.

The mentioned flow can be investigated by using numerical methods and/or by performing laboratory measurements on physical models i.e. hydraulic models which are attenuate replications of original dams (prototypes). For a typical gravity dam, both numerical and experimental analysis of seepage are presented and compared.

* Corresponding author. Tel.: + 385 51 265 900; fax: + 385 51 265 910
e-mail address: vanja.travas@gradri.hr

2 Physical model

The flow domain, here denoted by Ω , is defined by the space filled with porous material in the physical model illustrated on Fig. 2. The considered space region is rectangular with dimensions (length \times height \times thickness): 95 cm \times 30 cm \times 5 cm. Since there are no lateral inflows in the contained porous material, and the cross section area doesn't vary within the model, the transverse component of velocity is relatively small and can be neglected. As a consequence, the flow can be studied as a two-dimensional flow in a rectangular plane with length $l=95$ cm and height $h=30$ cm (Fig. 2).

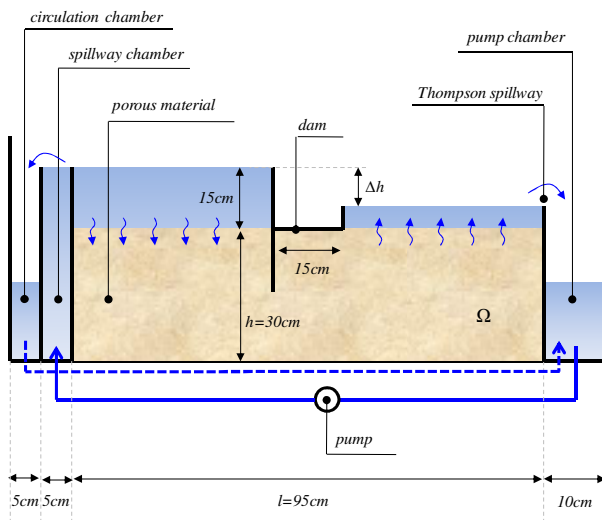


Figure 2. Cross section of the used physical model.

To activate a steady flow, the analysis of seepage for constant boundary conditions is carried out. In other words, relatively to the position of the dam and the direction of the flow, the upstream and downstream water levels are kept constant during the time of measurements. The water circulation through the domain Ω (porous material) is activated by inducing the pressure gradient between the inflow and outflow boundaries (Fig. 2). Between these boundaries, the Darcy law is valid [6,7]

$$\mathbf{v} = -\mathbf{K} \text{grad} (H) \quad (1)$$

where \mathbf{v} is the Darcy velocity vector, \mathbf{K} is the second order tensor of saturated permeability and H is the total head defined as

$$H = y + \frac{p}{\rho g} \quad (2)$$

in which y denotes the geodesic elevation of fluid particles (measured from the bottom surface of the model), p is the local pressure, ρ is the fluid density and g is the acceleration of gravity. Note that the total head H (2) represents the amount of mechanical energy per unit weight of a fluid particle. Namely, the magnitude of water velocity through the porous material is such that the contribution of kinetic energy can be neglected.

To obtain a homogeneous spatial distribution of porosity, the flow domain is everywhere filled with the same material. The material under consideration can be categorized as sand (on the upper limit of categorization) with granulation of $0.7\text{-}1.8 \text{ mm} \pm 0.3 \text{ mm}$. Indeed, for all cross sections of the porous structure, the ratios of material surface and voids have relatively small variations. In other words, the used sand can be treated as a statistically isotropic porous material. Under these circumstances, the permeability tensor \mathbf{K} is reduced to a scalar quantity, which was previously measured and identified to be $1.3 \pm 0.1 \text{ cm/s}$.

If the Reynolds number is considered, note that the characteristic flow velocity, which is around 4 cm/s in a flow domain (obtained by numerical analysis), the average pore size of $0.4 \pm 0.2 \text{ mm}$ and the classical mechanical properties of water will define Re equal to 9.1 . Accordingly, the steady flow in the physical model can be categorized as laminar flow for which the applicability of Darcy's law (1) is valid [8]. However, as can be noted, the used material is not opportune to steady seepage flow if the average flow velocity is greater than the one obtained in the physical model (in that case the Darcy equation will not be valid). On the other hand, the reason to choose such porous material is here mainly motivated by an intention to stimulate the process of local erosion at the tip of the dam foundation. As it is shown at the end of the paper, a particular set of boundary condition will induce the process of local erosion.

To induce the pressure gradient, an outside electric pump is used to subtract the water from the so-called *pump chamber* and pump it on the opposite side into the so-called *spillway chamber* (Fig. 2). Since the chamber has two spillways on/at the same height, a half of the pumped water is then released into the *circulation chamber* (introduced to ensure a

constant water level at the upstream side) and the rest is poured back into the upstream side of the model. This constant supply of water at the upstream side will enable a constant infiltration rate into the porous material. At the same time, the outflow of water through the downstream boundary is released back into the pump chamber. Therefore, once the outflow of water from the *pump chamber* has become equal to the inflow from the porous material, the steady flow is reached ($\partial v_i / \partial t = 0$). The water circulation inside the physical model is illustrated in Fig. 2.

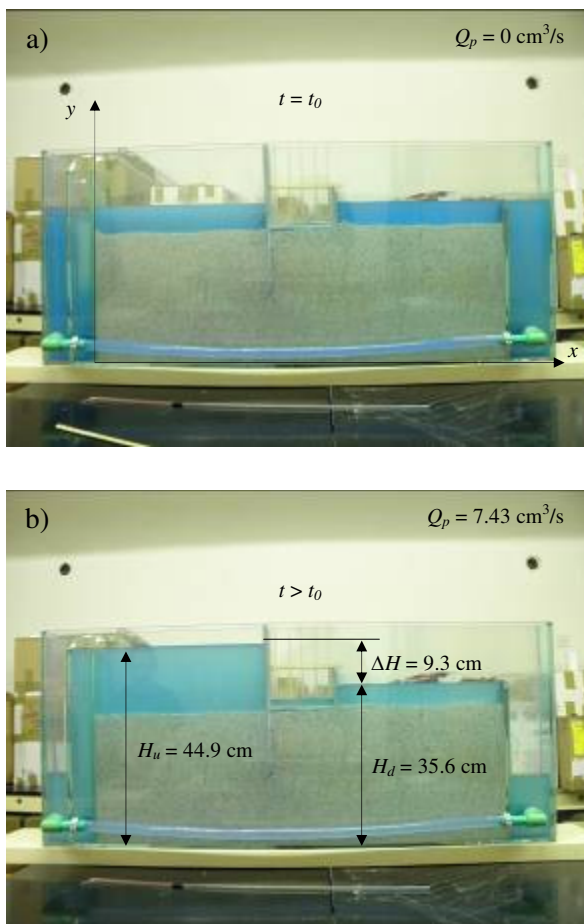


Figure 3. a) The initial standstill state and b) water levels for steady flow condition.

For the defined geometry and flow parameters, Fig. 3 illustrates the initial state and the reached steady flow. The steady flow is defined with the upstream water level $H_u = 44.9 \pm 0.1$ cm and the downstream level $H_d = 35.6 \pm 0.1$ cm. By correlating the spillway height with the discharge, the reached discharge Q_p is measured on/by a Thomson weir (Fig. 2) and indentified to be 7.43 ± 0.3 cm³/s.

To reduce the buoyancy at the bottom of the dam, a hydraulic barrier was embedded for 15 cm in depth. However, before performing any measurements, it was necessary to test the permeability of the barrier. The mentioned was done by injecting the dye near the barrier. Namely, since the particle trajectory coincides with the stream lines (as a consequence of steady flow), the dye injection will trace the local flow and show the presence of eventual permeable boundaries. As illustrated in Fig. 4, by bypassing the hydraulic barrier, the injected dye shows that the permeability condition is satisfied.

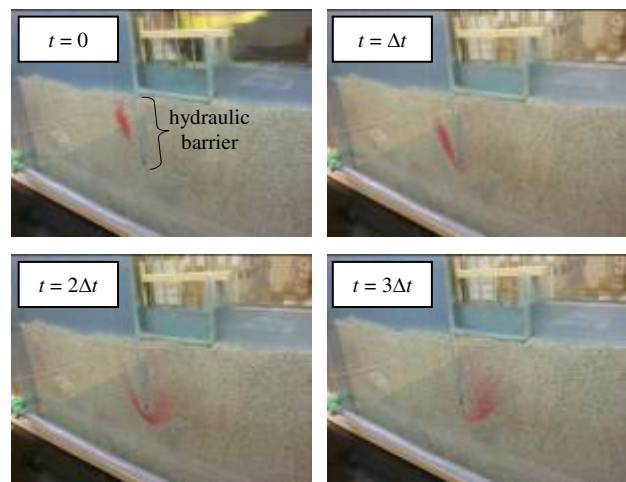


Figure 4. Sequence of photographs of a dye trajectory around the embedded hydraulic barrier.

The pressure p at an arbitrary point T in the flow domain is measured through $p = \rho gh$ i.e. indirectly by measuring water rise h in a piezometer placed at the point T . However, to isolate only the contribution of pressure to the water elevation, the measured water height h is afterwards reduced by the capillary rise h_c which for the used piezometers is indentified to be 4.0 ± 0.5 mm. Note that the measured water elevation h , reduced by h_c , is the second term in Eq. 2 (piezometer water elevation). A set of 5 piezometers (so-called *piezometric harp*) is used to measure the total buoyancy at the bottom of the model. By measuring the water elevation in each of them, the total vertical force U (buoyancy) is obtained by integration of the pressure

$$U = \sum_{i=1}^5 B(\rho gh_i) \Delta l_i \quad (3)$$

in which B is the width of the model, h_i is the water elevation in piezometer i (measured from the model foundation) and Δl_i is the local discretization length around the piezometer i . According to Eq. 3, the measured buoyancy is equal to 5.21 [N]. With respect to the considered scale of the flow, it is easy to agree that the obtained force is relevant. Namely, the obtained value is equivalent to a force produced on a floor by a mass of 0.53 kg, and at the same time the mass of the model of the dam (which was previously fixed) is around 0.25 kg.

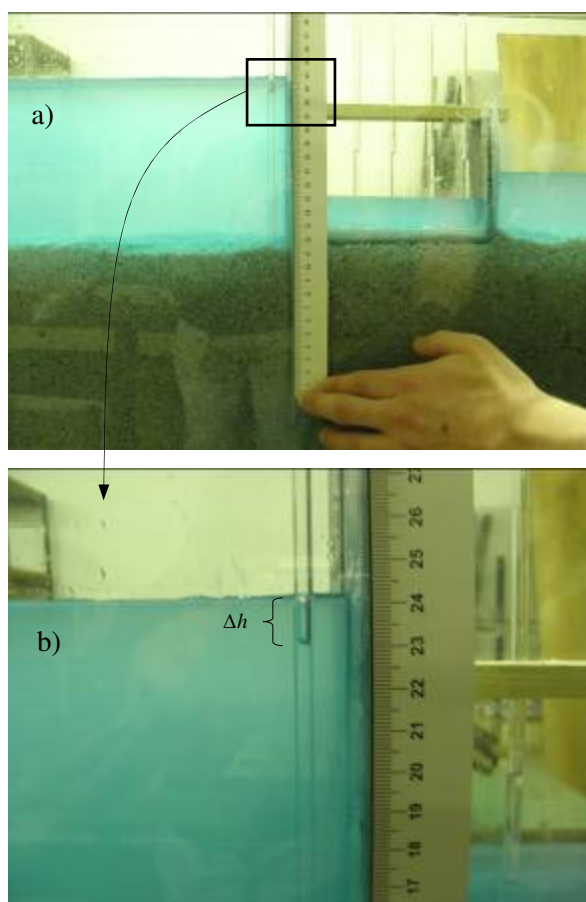


Figure 5. Measuring the pressure head at a point near the hydraulic barrier.

Apart from the buoyancy at the foundation, the pressure is also measured at a different depth along one side of the hydraulic barrier. Particularly, the pressure is measured only on the upstream side of the barrier, and this is because the other side (below the dam foundation) is unreachable by piezometers (Fig. 5).

By increasing the depth of the measurements along the hydraulic barrier, the pressure increases, but not according to the linear hydrostatic pressure

distribution. As shown in Fig. 5b, the measured pressure is smaller than the hydrostatic pressure calculated for the same depth. Indeed, by increasing the depth of measurements, the difference Δh (Fig. 5b) increases. By considering the transformation of water energy in the flow, it is easy to understand the origin of the evidenced difference. Namely, due to viscosity, Δh can be interpreted as an amount of energy (per unit weight of a fluid particle) used to overcome the resistance that the porous media provides from the point of infiltration to the point where the pressure is measured.

3 Numerical model

Since for the considered flow, the presence of vorticity can be neglected, which follows from the fact that the scale of vorticity is much smaller than the scale of the flow domain, the streamlines can be computed according to the potential flow theory [9]. In this case, the two dimensional vector field

$$\mathbf{v} = \begin{Bmatrix} v_x(x, y) \\ v_y(x, y) \end{Bmatrix}, \quad (4)$$

can be expressed through a gradient of a scalar field $H(x, y)$

$$\mathbf{v} = - \begin{bmatrix} K_x(x, y) & 0 \\ 0 & K_y(x, y) \end{bmatrix} \begin{Bmatrix} \frac{\partial H(x, y)}{\partial x} \\ \frac{\partial H(x, y)}{\partial y} \end{Bmatrix}, \quad (5)$$

which together with the continuity equation [5]

$$\frac{\partial v_x(x, y)}{\partial x} + \frac{\partial v_y(x, y)}{\partial y} = 0, \quad (6)$$

gives

$$\frac{\partial}{\partial x} \left(-K_x \frac{\partial H(x, y)}{\partial x} \right) + \frac{\partial}{\partial y} \left(-K_y \frac{\partial H(x, y)}{\partial y} \right) = 0. \quad (7)$$

Since the used porous material is isotropic

$$K_x = K_y = K, \quad (8)$$

and homogeneous

$$K \neq f(x, y), \tag{9}$$

Eq. (6) can be rewritten as

$$\frac{\partial^2 H(x, y)}{\partial x^2} + \frac{\partial^2 H(x, y)}{\partial y^2} = 0, \tag{10}$$

which is the well known Laplace equation. For the considered flow domain Ω , the function $H(x,y)$ can be approximated by numerical integration of Eq. (10). However, to achieve the same flow conditions as in the physical model (Fig. 2), as it is well known, the crucial «ingredient» is the correct specification of boundary conditions. Hence, since the considered flow is steady, it should be noted that the upstream infiltration boundary and the downstream outflow boundary are characterized by constant water levels on each side. In other words, on those boundaries, the Dirichlet type of boundary conditions should be defined by specifying the total head H (2), i.e. by H_u on the upstream side and H_d on the downstream side [6]. The other boundaries are impermeable and as such they are defined by the Neumann type of boundary conditions [6]. Therefore, the partial derivative of H perpendicular to the boundary is set equal to zero. Obviously, the dam foundation and the hydraulic barrier inside the flow domain Ω are also defined as impermeable boundaries. The specified boundary conditions are illustrated in Fig. 6.

To obtain an approximation of the scalar function $H(x,y)$, Eq. (10) is numerically integrated by a finite difference method [7]. The numerical algorithm was written to enable the change in spatial increments in both directions (Δx and Δy). The adequate number of cells was found by an iterative procedure and was acquired by compromising between the computational efficiency and the numerical accuracy of the obtained results. Accordingly, in x and y coordinate directions, the related special increments Δx and Δy are set to be 1 cm.

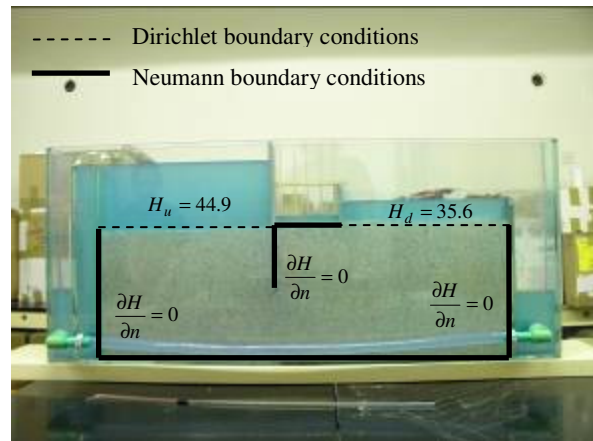


Figure 6. Boundary conditions in a flow domain.

Therefore, the spatial position of cells is defined with two positive integer numbers i and j . In each cell of the generated mesh, the scalar value $H_{i,j}$ is calculated respectively to the values of $H_{i\pm 1, j\pm 1}$ over the surrounding cells (11).

$$H_{i,j} = \frac{H_{i+1,j} + H_{i-1,j} + H_{i,j+1} + H_{i,j-1}}{4} \tag{11}$$

Particularly, depending on the relative position of each cell in the mesh and given boundary conditions (Fig. 6), a different contribution of surrounding values of H should be specified. The related equations can be found in the literature [7]. The mentioned will result in a formation of a system of linear equations. The resulting system is here solved iteratively by the method of *relaxation* [8,10]. The iterative procedure ends when in all computational cells the difference in $H_{i,j}$ between two neighborhood iterative steps k and $k+1$ becomes less than some predefined value δ (12).

$$\left| H_{i,j}^{k+1} - H_{i,j}^k \right| \leq \delta \tag{12}$$

The numerical algorithm is implemented in the program *MathCAD Professional 2001* [11] and used to retrieve the pressure field and the velocity field inside the porous material. For boundary conditions in Fig. 6, Fig. 7 shows the spatial distribution of total head $H_{i,j}$ (values interpolated between cells).

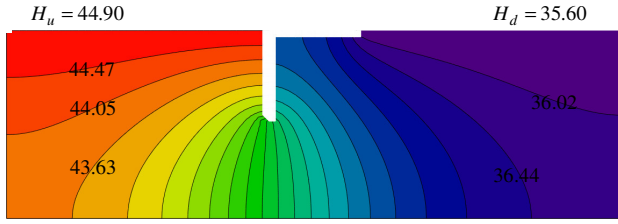


Figure 7. Scalar field $H(x,y)$ and equipotential lines

Since it is obvious that the geodetic elevation y of each point in the flow domain is known, according to Eq. (2) the now determinate field $H_{i,j}$ can be used to determinate the pressure in all the cells of the finite difference mesh. Thereby, to define the buoyancy, the pressure field is computed in all the cells below the dam foundation. The obtained pressure distribution is shown in Fig. 8. As it was expected, the pressure head on the downstream side of the dam foundation (Fig. 8) coincides with the water level H_d on the same side of the dam (Fig. 6).

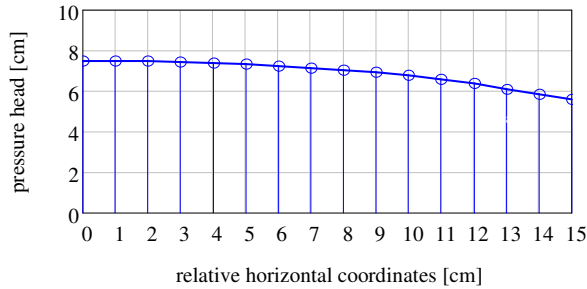


Figure 8. Pressure distribution on the foundation.

By integrating the pressure field in the same manner as in Eq. (3), it follows that the upward vertical force at the dam foundation is equal to 4.68 N, which is equivalent with a force produced on a floor by a mass of 0.47 kg.

Since the porous material is assumed to be isotropic (8) and homogeneous (9), the intersection between tangents on stream lines Ψ is always perpendicular to related tangents of equipotential lines H (Fig. 9). In other words, an arbitrary number of stream lines can be determined from Fig.7 [9].

The perpendicular relationship between stream lines and equipotential lines is an important feature of the considered physical process. Namely, since it is of interest for the later comparative analysis, it can be used to compute the flow discharge Q_n and compare it with the measured one in the physical model. For this purpose, an arbitrary number n of equidistant

streamlines Ψ (divided by some quantity $\Delta\Psi$) was traced upon the equipotential lines. By calculating the flow discharge Δq between two neighboring stream lines, the total discharge Q_n beneath the dam can be determined/defined as $\Sigma\Delta q$, where the summation index goes up to $n-1$. According to the Darcy law (1) and the geometrical specification given in Fig. 9, the elementary discharge Δq can be computed as

$$\Delta q = K \frac{\Delta H}{\Delta l} \Delta a \Delta b, \quad (12)$$

in which Δb denotes the thickness of the flow, ΔH denotes the drop in total head H (2) between the considered equipotential lines and Δl denotes the distance between the same equipotential lines. For a case of 6 stream lines: $\Delta a = 5 \pm 0.1$ cm, $\Delta b = 4 \pm 0.1$ cm, $\Delta l = 3 \pm 0.1$ cm and the drop in total head ΔH is $0,19 \pm 0.1$ cm. Congruently with Eq. (12), it follows that the flow discharge Q_n is equal to 9.64 ± 0.4 cm³/s, which is different from the measured Q_p by $\sim 23\%$.

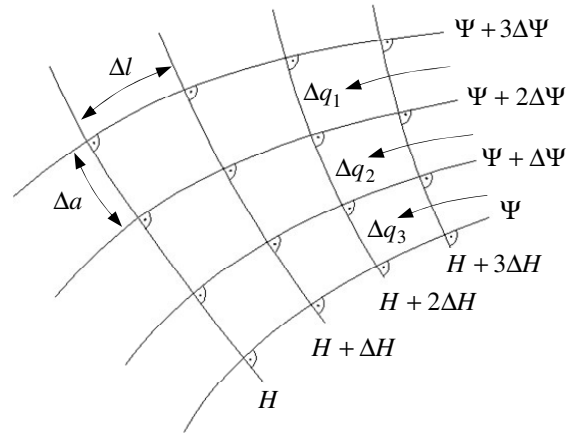


Figure 9. Equipotential and stream lines.

According to Eq. (5), by knowing K , the velocity vector field can be computed from the total head H . Thereby, the component v_x in a finite difference cell with coordinates (i,j) is approximated as

$$v_x = -K \frac{\partial H}{\partial x} \approx -K \left(\frac{H_{i+1,j} - H_{i-1,j}}{2\Delta x} \right), \quad (13)$$

and analogically, the v_y component is

$$v_y = -K \frac{\partial H}{\partial y} \approx -K \left(\frac{H_{i,j+1} - H_{i,j-1}}{2\Delta y} \right). \quad (14)$$

For a rectangular section of the flow domain Ω , defined around the hydraulic barrier and the foundation, the v_x and v_y velocity components are respectively illustrated in Fig. 10a and Fig. 10b. The specified velocity values are given in terms of cm/s. The maximal v_y component is 0.13 cm/s and, as expected, it is localized at the downstream tip of the dam foundation (Fig. 10b). At the same location, the v_x component is about 8 times greater. This is an interesting fact and suggests that the eventual manifestation of local erosion will not primarily cause the particle to lift but to drag apart. As shown hereafter, the experiments confirm this scenario.

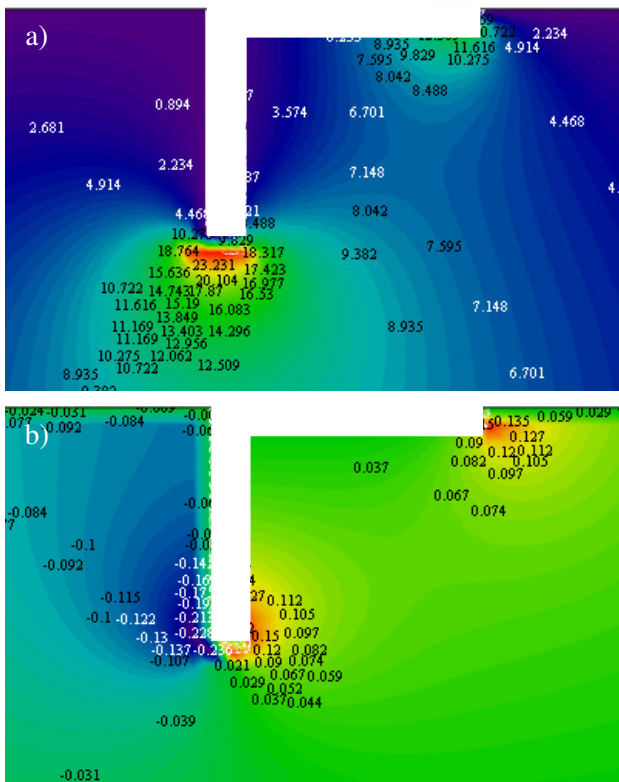


Figure 10. Scalar field a) v_x and b) v_y in cm/s.

4 Comparative analysis

Since it is very hard to measure the velocity at a point in the porous material, the velocity field in the physical model and the one obtained for same boundary conditions by numerical integration are compared qualitatively. For this purpose, it should be noted that for the obtained steady flow in the

physical model, the water particles trajectory coincides with the flow stream lines. This fact is used as an argument for tracing the local velocity field by dye injection. Accordingly, Fig. 10 shows the dye trajectory in three different positions and Fig. 12 the related vector field predicted at the same location by numerical integration of Eq. (10).

Note that on both side of a hydraulic barrier, the velocity vectors plotted in Fig. 12 are slightly inclined, i.e. they are not parallel to the solid boundaries of the hydraulic barrier. Of course, in these regions, the flow vectors are parallel to the hydraulic barrier and the illustrated slightly inclined directions are a consequence of spatial discretization and arise from the fact that the computational grid cells are shifted away by Δx from the considered soil boundary.

By comparing the dye trajectory (Fig. 11) with the relevant velocity vectors field in Fig. 12, it can be deduced that the numerical model correctly predicts (at least qualitatively) the velocity field. However, it is the most interesting to focus on Fig. 12c, which shows a detailed view of the vector field in the zone that is a candidate for local erosion. Namely, note that the angle of the velocity vector at the tip of a dam foundation (Fig. 12c) is equal with the angle of a dye jet at the exit of the porous material in the same region (Fig. 11c). Although the process of local erosion was not evidenced in the physical model, the orientation of velocity vectors shows the tendencies to lift the soil particles by the induced hydrodynamic force on them. To test if the process of local erosion can occur, a set of different boundary conditions was tested. Particularly, the one which will generate the maximal velocity at the outflow is the one with the maximal upstream water level H_u and minimal downstream water level H_d (max ΔH). Indeed, with such boundary conditions, the local erosion was obtained (Fig. 13).

Before introducing an interesting note into the analysis of the evidenced local erosion (Fig. 13), it is worth pointing out that the geometry of stream lines doesn't change by changing the magnitude of H specified on the Dirichlet type of boundary conditions. The only thing that will change as a consequence of different water levels on the upstream and downstream side of the model is the magnitude of velocity. In other words, both velocity components will be scaled up with the same factor, retaining the direction of the velocity vector. The

mentioned is a consequence of the fact that the flow domain is always the same.

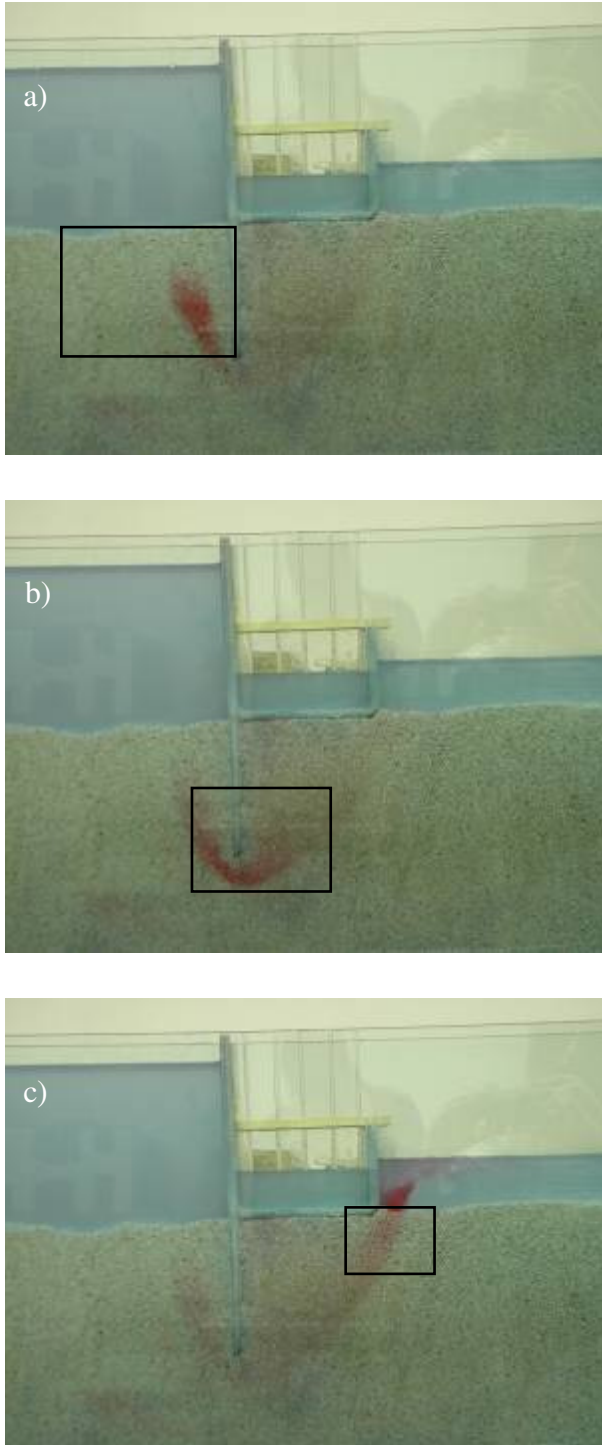


Figure 11. Evidenced stream lines by dye injection.

Nevertheless it is opportune to recall the velocity field illustrated in Fig. 10. Namely, as it was commented earlier, the documented local erosion is

characterized by a dominant dragging of particles and not by lifting up the soil particle. And the magnitude of the horizontal components of velocity was identified to be 8 times greater than the vertical components in the region where the local erosion was recorded.

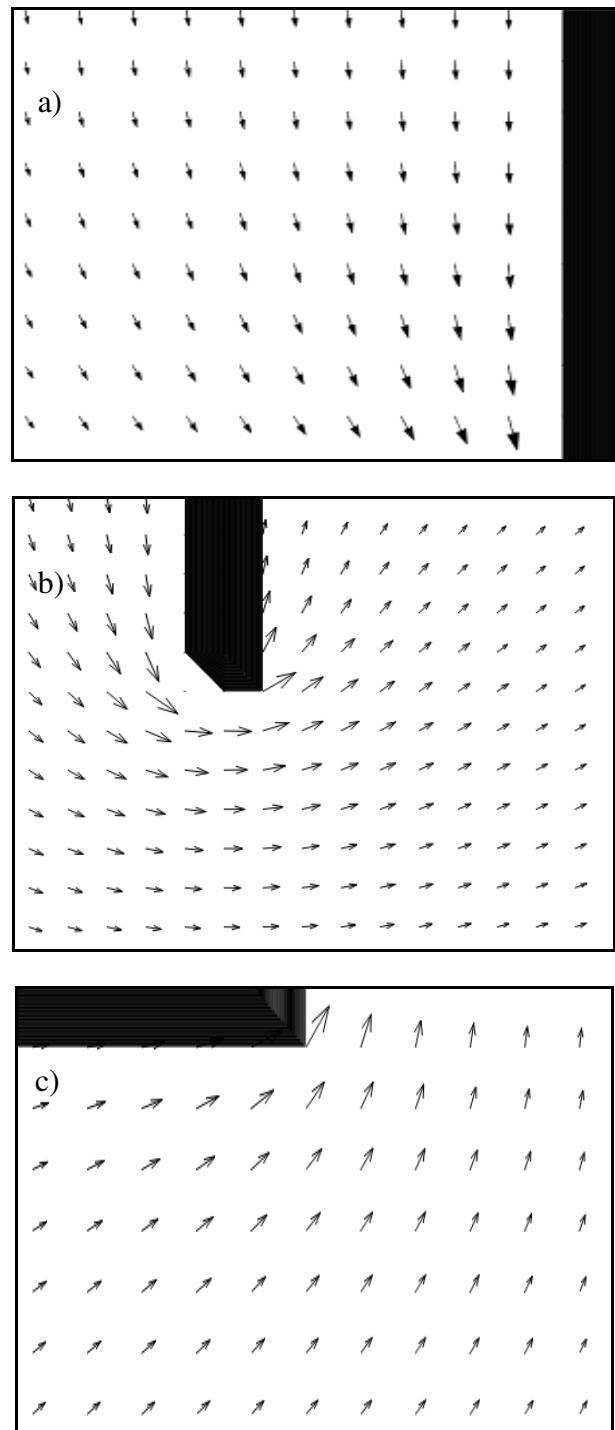


Figure 12. Segments of velocity field around the dam.

It is very important to note that the conventional numerical models of seepage, that are only based on solving the Laplace equation (as here presented) cannot be used to predict local erosion.

Also, note that once the process of local erosion occurs, the velocity field locally changes in time as the particles are dragged apart from the porous material. In other words, to simulate the evolution of consequences caused by local erosion, an unsteady description of the flow is needed.

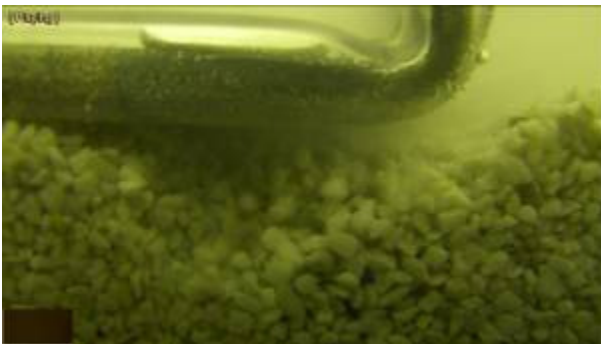


Figure 13. Local erosion at the tip of the foundation

An idea to simplify the numerical description of a complex phenomenon of local erosion is hereafter briefly presented. Namely, note that the change in the velocity field can be locally imposed just by specifying an appropriated saturated permeability K (1). To describe that as a function of particles dragging apart, the mentioned requires an additional phenomenological equation that will relate the actual velocity field with the amount of particles dragged apart by local erosion. Obviously, this relationship should be given in terms of geometrical and mechanical properties (density) of the porous material. By performing a set of parametric analysis on the physical model, the relationship should be defined by regression. So, for the given flow field obtained by numerical integration of Eq. (10), at the tip of the dam foundation, a phenomenological criteria for local erosion are tested in each cell. After that, if the phenomenological model predicts particles moving, an accordingly increasing in saturated permeability K is calculated. By updating the distribution of saturated permeability K , a new prediction of the velocity field is computed. The iterative process is performed in time until a steady flow conditions have been obtained. The described idea is based on a set of relatively simple quasi-coupling of two fields and will be examined in some future work.

Apart from the computed velocity field (Fig.12), which shows a good concurrence with the same field in the physical model, the measured Q_p and computed flow discharge Q_n was different for about 23%. The first thing that should be mentioned to explain such a difference is that the measured flow discharge Q_p was determined by relating it with the water level h_t on a Thomson weir (which was measured for a flow direction perpendicular to the weir) [1]. For that reason, and as a consequence of small measuring environment, it was inevitable to exclude the present contribution of capillary effects on the total water elevation h_t (which is, by way of contrast, easy to do for a capillary tube). On the other hand, the computed and measured pressure field on the dam foundation, i.e. the buoyancy was different for $\sim 10\%$. The origin of this distinction can be prescribed to the relatively small number of piezometers on the dam foundation. Namely, note that the buoyancy is obtained by integration of the pressure field, which was known in 15 positions for a case of a numerical model and 5 positions for the physical model. The obtained difference can be a consequence of this different discretization of the pressure field.

5 Final remarks

A comparative analysis between a physical process of seepage beneath a model of a gravity dam and the related numerical predictions of the same process is performed. The physical model is constructed at the Faculty of Civil Engineering at the University of Rijeka and was previously tested whether it can ensure controlled experimental conditions. On the other hand, the numerical model of seepage was implemented in *MathCAD 2001 Professional* and was used to retrieve the numerical predictions of the flow in the same domain and with the same boundary conditions, which was specified by total head H on the upstream and downstream part of the dam. A qualitatively comparative analysis between the velocity fields shows a good agreement. However, a difference between the flow discharge and the buoyancy was obtained and was probably caused by errors included in the measurements. A particularly interesting phenomenon of local erosion was obtained for the most adverse combination of boundary conditions. Since such a process is of great importance to this research, an idea to include the phenomenon in the numerical description is

presented. Namely, as previously described, some future work will primarily consist of examining the possibility of relating the criteria for local erosion to the velocity field. Apart from the mentioned, it will be also interesting to examine the functional relationship between the drop in buoyancy by increasing the depth of the hydraulic barrier. However, for this purpose, a modification on the model of the dam should be made.

List of symbols

H	total head
\mathbf{K}	permeability tensor
K_x	permeability in x direction
K_y	permeability in y direction
p	local pressure
ρ	density
H_u	upstream water level
H_d	downstream water level
B	width of the physical model
Δl_i	local discretization length
h_c	capillary rise in piezometri tube
\mathbf{v}	velocity vector
v_x	x component of velocity vector
v_y	y component of velocity vector
Ω	flow domain
Δh	difference in water level
δ	criteria for convergence
k	iterative step counter
i, j	discrete coordinates in a FD mesh
Δx	spatial increment in the x direction
Δy	spatial increment in the y direction
Ψ	stream function
n	number of stream lines
Q_n	computed discharge
Q_p	measured discharge
Δq	elementary discharge

References

- [1] Horton, R.E.: *Weir experiments, coefficients and formulas*, Water-Supply and Irrigation, 1951, Paper No. 200.
- [2] Kodaka, T., Oka, F., Morimoto, R.: *Seepage failure analyses of sandy ground using a liquefaction analysis method based on finite deformation theory*, The first Asian-Pacific Congress on Computational mechanics, Sydney, Australia, 2001, 387-392.
- [3] Sitharam, T.G., Dinesh, S.V.: *Numerical simulation of liquefaction behaviour of granular materials using Discrete Element Method*, Proceedings of the Indian Academy of Sciences (Earth Planet Sciences), 112 (2003), 3, 479-484.
- [4] Snieder, R., van den Beukel, A.: *The liquefaction cycle and the role of drainage in liquefaction*, Granular Matter, 6 (2004), 1-9.
- [5] Crosta, G., di Prisco, C.: *On slope instability induced by seepage erosion*, Canadian Journal of Geotechnics, 36(1999), 1056-1073.
- [6] Bear, J.: *Hydraulics of groundwater*, McGraw-Hill, New York, 1979.
- [7] De Wiest, R.J.M., Bear, J.: *Flow through porous media*, Academic Press, New York, 1969.
- [8] Bear, J., Cheng, A.H.-D.: *Modeling groundwater flow and contaminant transport*, Springer, Berlin, 2010.
- [9] Matovic, D.: *Stream function, vorticity and velocity potential*, course notes, Department of Mechanical and Materials Engineering, Queen's University, 2010.
- [10] Bear, J.: *Dynamics of fluids in porous media*, American Elsevier Publishing Company, New York, 1988.
- [11] *Mathcad User's Guide with Reference Manual Mathcad 2001i*, MathSoft Engineering & Education, Inc., Cambridge, MA 02142, 2001.